Combined MAM-PCA autofocus for stripmap SAR

Rifat Afroz*, Brian Ng, Derek Abbott
School of Electrical and Electronic Engineering
The University of Adelaide
Adelaide, SA 5005, Australia
*rifat.afroz@adelaide.edu.au

Rolf Scheiber
Microwaves and Radar Institute
German Aerospace Center (DLR)
Oberpfaffenhofen-Wessling, Germany

***Abstract*—The nonparametric phase curvature algorithm (PCA) is commonly used to estimate residual motion error in stripmap SAR. The algorithm is capable of estimating second and higher order errors, as well as high frequency errors. However, its dependence on dominant scatterers restricts its application to a wide variety of scenes. Such a limitation is encountered in focusing a polarimetric L-band SAR dataset collected from an agricultural field. The lack of dominant scatterers in the scene results in inaccurate error estimation when PCA is applied directly. Another autofocus scheme, the Multi-aperture Mapdrift (MAM), is used first to eliminate the low order motion errors. This improves the focusing quality of the existing targets. The enhanced point targets are then suitable for PCA to remove the remaining higher order motion errors. The novel MAM-PCA combination significantly improves the image contrast compared to that obtained from the approaches applied separately. Point target based comparison of MAM, PCA and MAM-PCA show that the proposed technique improves the overall quality of the target profile.**

***Index Terms*—Stripmap, synthetic aperture radar (SAR), motion compensation (MOCO), autofocus, multi-aperture mapdrift (MAM), phase curvature algorithm (PCA).**

I. Introduction

Airborne synthetic aperture radar (SAR) data usually require motion compensation (MOCO) before image formation in order to achieve its system-defined resolution. In practice, SAR systems that are equipped with highly accurate inertial navigation sensors (INS) for measuring the platform position to at least $\frac{\lambda}{8}$ precision [1] can simply rely on the sensor data for MOCO. Otherwise, a data-driven autofocus algorithm is required to eliminate the residual error [2].

For stripmap SAR, nonparametric phase curvature autofocus (PCA) is commonly used [3]. As a slightly modified version of the phase gradient autofocus (PGA), PCA offers estimation of both low and high frequency motion errors, including quadratic and higher orders [4]. However, similar to PGA, PCA relies on dominant scatterers in the SAR scene for the estimation process [5]. This makes the algorithm redundant for the scenes where dominant scatterers are scarce such as agricultural fields.

A viable autofocus option for such rural landscapes is the parametric mapdrift autofocus (MD). The algorithm does not depend on point-like targets. Distributed objects, i.e. trees, crops can rather be used for its estimation process [6]. As MD based estimation is limited only to the quadratic error, an advanced version known as the multi-aperture mapdrift (MAM) is proposed by Calloway et al. [6]. Here, MAM can reliably estimate high order errors that vary slowly. As the frequency of the error increases, the estimation becomes unreliable. Moreover, high order error estimation requires the aperture to be divided into large number of subapertures, which reduces the energy and resolution per sub-image [7]. Hence, MAM is ineffective in estimating high frequency and high order errors.

In order to estimate high order motion error with scarce targets in rural scenes, this work combines both the PCA and MAM. Combination of parametric and nonparametric autofocus can be found in the existing literature. Notably, MD and PGA are cascaded by Jin et al. [4] to compensate the residual range cell migration (RCM) in squint SAR. MAM, weighted PGA and contrast-optimization (CO) based autofocus are combined to compensate the residual RCM, along-track velocity and range-dependent phase error [7]. The MD-based approach is used to estimate unknown linear error in sub-aperture based PGA and extract residual RCM [8]. Modifications are made to PCA to improve its error estimation using Kalman filter [9] and extracting prominent points in the scene and applying adaptive window on them [3]. Weighted PCA is proposed to take the range-dependent nature of the phase error into account [2]. None of the above works combine MAM with PCA to improve the image quality first.

Due to the complementarity of the two algorithms, this work chooses to combine them. MAM is used to estimate the low frequency and low (up to third) order errors and PCA is used to estimate the low frequency higher order (greater than third) and high frequency components. The MAM method achieves sufficient enhancement of targets to allow PCA to work, thus estimating a larger range of errors than either method is individually capable of. Details of the novel MAM-PCA are given in Section II along with the overviews on MAM and PCA. Experimental results are discussed in Section III, which is followed by the conclusion.

II. Combination of MAM and PCA

A. MAM

An extension of the traditional MD, MAM is designed to estimate motion errors of order quadratic or higher [6]. It divides the entire aperture into a number of sub-apertures commensurate with the error order and estimates the error coefficients for each sub-aperture. The estimated coefficients

978-83-956020-4-7 ©2022 Warsaw University of Technology
IRS-2022,Gdańsk, Poland

are used to formulate the phase error over the full aperture. The azimuth phase error for flight duration T can be given as,

$$\phi_e(t) = \sum_{n=2}^{N} a_n t^n, \quad -\frac{T}{2} \leq t \leq \frac{T}{2}, \tag{1}$$

where a_n represents the coefficient of the error polynomial.

The aperture is divided into a number of nonoverlapping subsections equal to the highest error order N to be estimated. The error for each sub-aperture n can then be represented as the windowed version of (1) as [8],

$$\phi_{e,n}(t) = \phi_e(t) \operatorname{rect}\left(\frac{t - nT_n}{T_n}\right), \tag{2}$$

where T_n is the subaperture duration.

A crucial consideration while dividing the subaperture is that it has to be small enough to approximate the phase error to be linear. Therefore, it is sensible to measure only a linear drift caused by $\phi_{e,n}(t)$ within the sub-image. The drift is measured by correlating the image pairs and computing the correlation peak shift from the middle of the correlation index.

The linear shift between image pairs u and v can be associated with the error coefficient using the following relation:

$$\delta_{u,v} = \sum_{n=2}^{N} n a_n (t_u^{n-1} - t_v^{n-1}). \tag{3}$$

A matrix inversion is performed to estimate a_n from (3). The estimated a_n is then used to model the phase error using,

$$\hat{\phi}_e(t) = \sum_{n=2}^{N} \hat{a}_n t^n. \tag{4}$$

With the approach above, MAM can reliably estimate the motion error of quadratic or higher in order. However, the reliability is limited to low-frequency motion error only, as the linear approximation is not valid when the error frequency is high [6]. The other disadvantage of MAM is that if higher order error is to be estimated, the sub-aperture number increases proportionately. More sub-apertures mean lower resolution and less energy for each of them [7]. The measured drift becomes unreliable as a consequence. This limits the reliability of MAM in estimating high frequency error and very high order errors. Sinusoidal models instead of the polynomial model in (4) can improve high frequency error estimation. However, large sub-aperture division cannot be avoided even in that case.

B. PCA

The PCA algorithm is an adaptation of PGA for stripmap SAR [2]. It inherits the basic PGA assumptions, i.e. the phase error is range-invariant and dominant scatterers are abundant in the scene [10]. The first assumption enables using the maximum-likelihood (ML) estimator to combine the phase error estimates obtained from different range bins and the latter allows inclusion of multiple range bins in the estimation process. Similar to PGA, it starts by selecting the brightest pixels in the scene and windowing them. The windowed image is then decompressed and deramped to obtain the range compressed data. Using the deramped data, the phase difference among the neighbouring pixels is computed and summed over the range bins. The angle of this expression is the estimated phase curvature. The ML estimator for PCA is [2],

$$\hat{\dot{\phi}}_e(l) = \angle \sum_{k=1}^{K} g_{k,l-\Delta l} (g_{k,l}^*)^2 g_{(k,l+\Delta l)}, \tag{5}$$

where g is the deramped signal and k and l are the range and azimuth bins, respectively.

The curvature in (5) is then double integrated to obtain the phase error estimate. Unknown bias and linear terms are removed via line fitting the estimated phase error. The flowchart in Fig. 1b outlines the steps for the PCA.

As the autofocus relies on the dominant scatterers only to estimate phase error, ideally the error of any order (equal or higher than quadratic) and frequency retained by the target should be captured by PCA. However, dominant targets should be abundant (at multiple range bins across the swath) and they should be free from any other defocusing than the azimuth phase error. It also requires high SNR for the scene similar to PGA [4]. Therefore before applying PCA, the quantity and quality of the targets need to be ensured.

C. Combined MAM-PCA autofocus

As MAM can estimate low order errors and PCA can estimate high order and high frequency errors using dominant scatterers, we propose combining these two approaches to estimate errors of different orders and frequency for the scenes that have sparse dominant scatterers. The flowchart of the combined approach is shown in Fig. 1. It largely preserves the inherent structure of each algorithm and cascades them to utilize their individual merits. In MAM, the sub-images are oversampled to obtain the drifts at sub-pixel level. The low order and low frequency blurring components (second and third) are estimated by this block in Fig. 1a. Coarse motion compensated images are decompressed using the technique proposed by Wahl et al. [5] and the MAM estimated residual error is compensated via phase multiplication with it. When the root mean square (rms) error exceeds a threshold $e_{\mathrm{MAM,th}}$ the algorithm stops, assuming no further low order error is present. Then the PCA block in Fig. 1b estimates any higher order errors. The range-independent version of the PCA is used as the target scene that does not contain abundance of targets. The computed phase curvature is unwrapped to recover the integer multiples of 2π and then double integrated to estimate the remaining phase error. The MAM corrected image is deramped and compensated for the PCA estimated error via phase multiplication. A stopping criterion $e_{\mathrm{PCA,th}}$ is set for this block as well. An RMS error of less than $\frac{\pi}{4}$ can generally be set as the stopping criterion [11].

III. Experimental Results

In order to validate the performance of MAM-PCA autofocus, data from a Polarimetric L-band SAR (PLIS) are used. The parameters are in Table I. Along with radiometers, PLIS

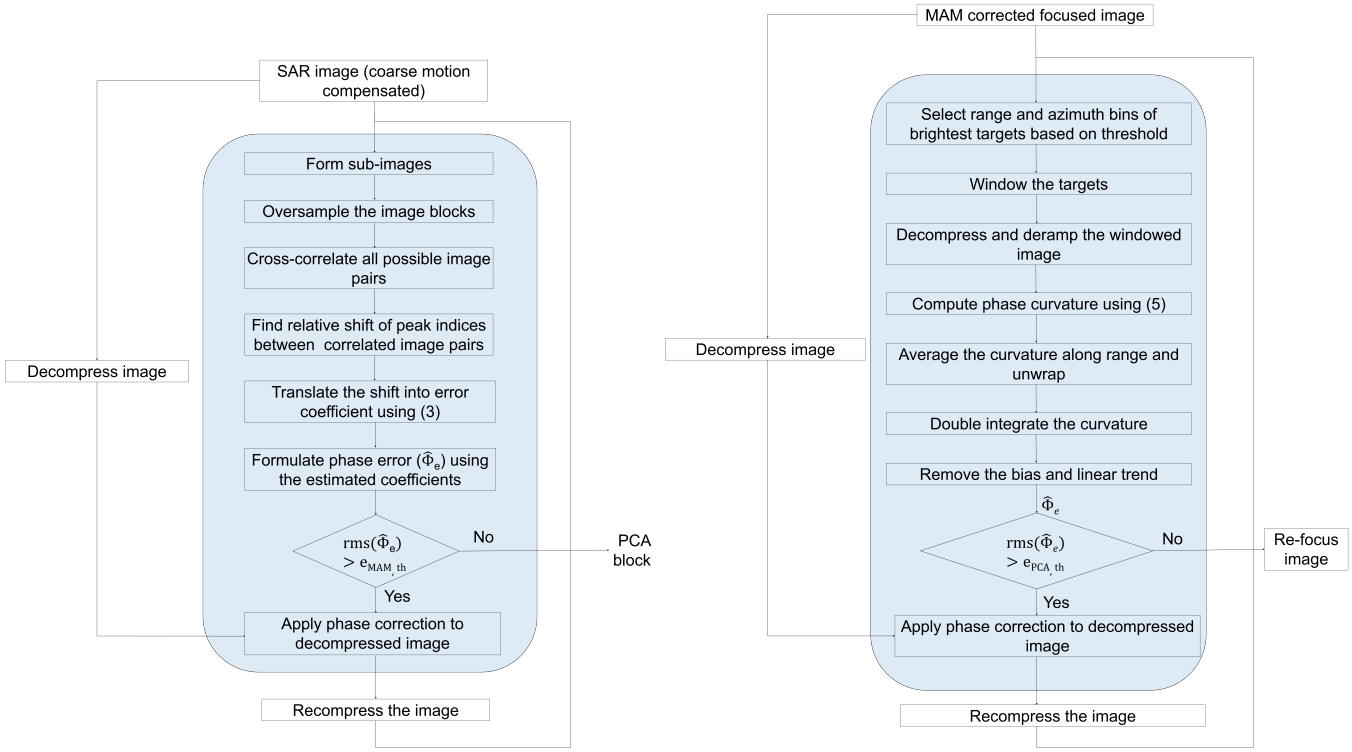

(a) MAM Block (b) PCA Block

Fig. 1: MAM-PCA based autofocus

system is deployed to validate NASA's soil moisture active passive (SMAP) mission [12]. In this trial, agricultural fields are the scenes of interest. The radar is flown in a light aircraft, making it more susceptible to large flight path deviations. Notably, a maximum of $20\,\text{m}$ deviation in the translational path is recorded as shown in Fig. 2. Position measurement accuracy of the INS is $1.5\,\text{m}$ [13], which is far from meeting the $\frac{\lambda}{8}$ accuracy requirement. The position update rate for the sensor is approximately 60 times lower than the radar's data rate. Thus autofocus is necessary to improve the focusing.

TABLE I: PLIS parameters

Centre frequency	$1.26\,\text{GHz}$
Range bandwidth	$30\,\text{MHz}$
Azimuth beamwidth	$51\,\text{deg}$
Azimuth resolution	$0.57\,\text{m}$
PRF	$625\,\text{Hz}$
Nominal velocity	$76.4\,\text{m/s}$
Swath width	$2.2\,\text{km}$

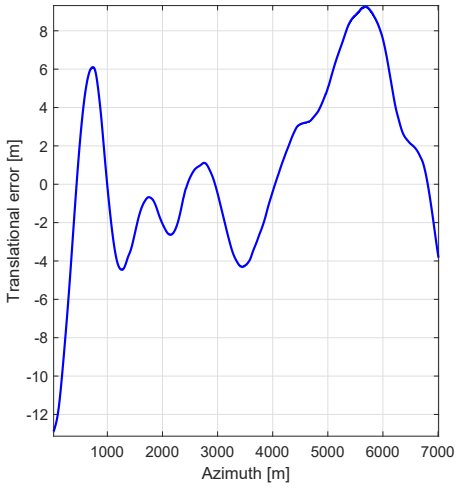

Fig. 2: LOS error extracted using INS data

A definite error order is not known to parameterize a model. But intuitively it can be said from the translational deviation in Fig. 2 that the residual error may have higher (than quadratic) order and fast varying ($> \frac{1}{\text{aperture time}}$) components. PCA can be particularly suitable for such problems. Due to the lack of good quality point-like targets in the scene, PCA cannot be applied directly, however. Therefore, MAM is applied to the scene first. A third order MAM is chosen as target blurring occurs due to the errors of up to cubic [6]. This enhances the image by sharpening the point-like features. The enhanced point-like features are then used to estimate the residual error of order higher than cubic using the PCA. Two good quality targets are used for the PCA estimation. Only a single iteration is performed for each block as the error converged after that.

The difference in the estimated error and their usefulness in improving the images are evident in Fig. 3. A coarse motion compensated and MD corrected image in Fig. 3a is utilized in this work. A third order MAM is applied

to this scene. Improvements, compared to the original, are particularly noticeable from rectangles A and B in Fig. 3b. Here, MAM improves the mainlobe of the point-like features in with slight increase in the sidelobes. This is due to the residual error of higher order present in the original scene that could not be parameterized in MAM without prior knowledge. Compensating the errors by applying the nonparametric PCA directly to the original scene blurs it further as the targets used for its estimation were not of good quality. This effect can be seen in Fig. 3c. In contrast, significant improvements are obtained using the MAM-PCA as apparent in Fig. 3d. By retaining the enhanced mainlobe feature from MAM, the combined approach allows a proper execution of PCA. As the latter is not limited to any error order, it improves the image quality by suppressing the sidelobes that originated from higher order errors. Standard deviation intensity contrast function given by Berizzi et al. [14] are computed for the scenes. While the MAM and PCA corrected scene contrasts are 20.85 and 18.53, respectively, MAM-PCA corrected scene is 29.42.

A point-like feature at range $674\,\mathrm{m}$ is extracted and compared in Fig. 4. It can be seen that both MD and MAM improves the mainlobe of the target by compensating the quadratic and cubic errors respectively. On the other hand, PCA alone improves the sidelobe relatively as it used blurred targets for the estimation process. When combined, the benefit of both the approaches is availed and the overall PSF of the target is improved. PSF parameters for the target obtained from the four approaches are given in Table II.

The proposed technique can be made suitable to higher frequency (than L-band) SAR systems as well where the severity of motion error is worse [7]. Increasing the order of MAM and using the weighted version of PCA [2] will enable MAM-PCA to handle severe errors that are also range-dependent.

TABLE II: Comparison among MD, MAM, PCA and MAM-PCA

Approach	3dB width [m]	PSLR [dB]	ISLR [dB]
MD	1.46	- 4.90	-14.70
MAM	**0.91**	-1.82	-7.26
PCA	1.98	-6.97	**-20.22**
MAM - PCA	**0.91**	**-9.12**	-12.12

IV. Conclusion

Stripmap SAR scenes affected with a combination of low and high order and frequency errors can ideally be compensated with nonparametric PCA autofocus. However, if the scene does not provide sufficient dominant scatterers, PCA cannot be applied directly. Correcting the image with parametric MAM in these cases can make PCA application possible by sharpening the existing point-like features. In this work, a combined MAM-PCA autofocus is used to improve the image contrast significantly. Comparison of the three approaches is made. It is found that the combined approach can improve the overall PSF quality.

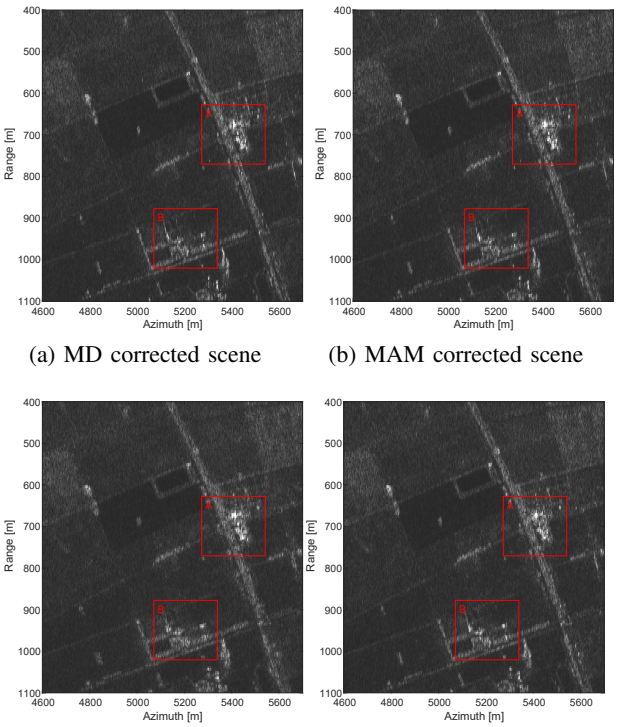

(a) MD corrected scene (b) MAM corrected scene

(c) PCA corrected scene (d) MAM-PCA corrected scene

Fig. 3: Agricultural scene improvement via MAM-PCA

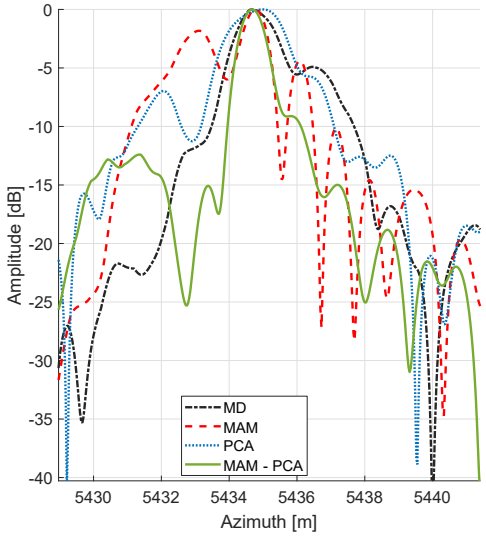

Fig. 4: PSF improvement via MAM-PCA approach

REFERENCES

[1] J. Svedin, A. Bernland, and A. Gustafsson, "Small UAV-based high resolution SAR using low-cost radar, GNSS/RTK and IMU sensors," in *2020 17th European Radar Conference (EuRAD)*, 2021, pp. 186–189.

[2] K. A. C. de Macedo, R. Scheiber, and A. Moreira, "An autofocus approach for residual motion errors with application to airborne repeat-pass SAR interferometry," *IEEE Transactions on Geoscience and Remote Sensing*, vol. 46, no. 10, pp. 3151–3162, 2008.

[3] J. Saeedi, "Improved phase curvature autofocus for stripmap synthetic aperture radar imaging," *IET Signal Processing*, vol. 14, no. 10, pp. 812–822, 2020.

[4] Y. Jin, J. Chen, X.-G. Xia, B. Liang, Y. Xiong, Z. Liang, and M. Xing, "Ultrahigh-resolution autofocusing for squint airborne SAR based on cascaded MD-PGA," *IEEE Geoscience and Remote Sensing Letters*, vol. 19, pp. 1–5, 2022.

[5] D.E. Wahl, C.V. Jakowatz, P.A. Thompson, and D.C. Ghiglia, "New approach to strip-map SAR autofocus," in *Proceedings of IEEE 6th Digital Signal Processing Workshop*, 1994, pp. 53–56.

[6] T. M. Calloway, *Automatic focus and registration of syntheic aperture radar images*, The University of New Mexico, 1992.

[7] J. Li, J. Chen, P. Wang, and O. Loffeld, "A coarse-to-fine autofocus approach for very high-resolution airborne stripmap SAR imagery," *IEEE Transactions on Geoscience and Remote Sensing*, vol. 56, no. 7, pp. 3814–3829, 2018.

[8] D. Zhu, R. Jiang, X. Mao, and Z. Zhu, "Multi-subaperture PGA for SAR autofocusing," *IEEE Transactions on Aerospace and Electronic Systems*, vol. 49, no. 1, pp. 468–488, 2013.

[9] Y. Li and S. O'Young, "Kalman filter disciplined phase gradient autofocus for stripmap SAR," *IEEE Transactions on Geoscience and Remote Sensing*, vol. 58, no. 9, pp. 6298–6308, 2020.

[10] H. L. Chan and T. S. Yeo, "Noniterative quality phase-gradient autofocus (QPGA) algorithm for spotlight SAR imagery," *IEEE Transactions on Geoscience and Remote Sensing*, vol. 36, no. 5, pp. 1531–1539, 1998.

[11] I. G. Cumming and F. H. Wong, *Digital Processing of Synthetic Aperture Radar Data: Algorithms and Implementation*, Artech House, Norwood, MA, 2005.

[12] L. Zhu, J. P. Walker, N. Ye, C. Rüdiger, J. M. Hacker, R. Panciera, M. A. Tanase, X. Wu, D. A. Gray, N. Stacy, A. Goh, H. Yardley, and J. Mead, "The polarimetric L-band imaging synthetic aperture radar (PLIS): Description, calibration, and cross-validation," *IEEE Journal of Selected Topics in Applied Earth Observations and Remote Sensing*, vol. 11, no. 11, pp. 4513–4525, 2018.

[13] Oxford Technical Solutions Ltd., *RT User Manual - OxTS*, 2021.

[14] F. Berizzi and G. Corsini, "Autofocusing of inverse synthetic aperture radar images using contrast optimization," *IEEE Transactions on Aerospace and Electronic Systems*, vol. 32, no. 3, pp. 1185–1191, 1996.